Marine Geology 451 (2022) 106866

Contents lists available at ScienceDirect

Marine Geology

journal homepage: www.elsevier.com/locate/margo

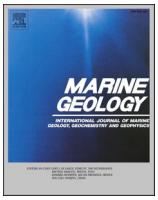

Do tidal sand waves always regenerate after dredging?

Janneke M. Krabbendam [a,*], Marc Roche [b], Vera R.M. Van Lancker [c], Abdel Nnafie [a], Nathan Terseleer [c], Koen Degrendele [b], Huib E. De Swart [a]

[a] Institute for Marine and Atmospheric research Utrecht, Utrecht University, Princetonplein 5, 3584, CC, Utrecht, the Netherlands
[b] Continental Shelf Service, Federal Public Service Economy, S.M.E.s, Self-Employed and Energy, Boulevard du Roi Albert II, 16, 1000, Brussels, Belgium
[c] Operational Directorate Natural Environments, Royal Belgian Institute of Natural Sciences, Vautier Street 29, B-1000, Brussels, Belgium

ARTICLE INFO

Editor: Shu Gao

Keywords:
Tidal sand waves
Recovery after dredging
Shelf morphology and stratigraphy
Field observations
North Sea
Europe

ABSTRACT

Tidal sand waves are rhythmic bedforms found on sandy continental shelves that pose a threat to offshore activities. While emphasis is placed on studying their natural morphodynamic evolution, little is known about if and how fast sand waves recover after dredging. This work presents an analysis of multibeam echosounder data collected at three former sand extraction sites on the Belgian continental shelf. At one of the sites, sand waves seemed to reappear approximately 5 years after dredging had stopped, which did not happen at the other two sites during the measurement period (5 and 9 years). The lack of recovery in those sites is likely the result of larger depths and smaller local sediment availability compared with the site where recovery occurred. Furthermore, these data reveal that in the latter site sand wave recovery was established mainly through local sediment redistribution.

- Tidal sand waves are isolated from bathymetric data of the Belgian continental shelf.
- At only one of the three sites, sand waves seemed to regenerate after dredging.
- Possible explanations are differences in water depth and local sediment availability.
- The regenerating tidal sand waves do so as a result of local redistribution of sand.

1. Introduction

Tidal sand waves, sometimes referred to as large to very large dunes (Ashley, 1990), are rhythmic bedforms with wavelengths of hundreds of meters, heights of several meters and they migrate over the sandy bed of continental shelf seas at rates of 1–10 m per year (McCave, 1971; Damen et al., 2018). They form spontaneously as a free instability of an oscillating tidal current interacting with an erodible bed (see the review of Besio et al., 2008). Tidal sand waves are often observed together with larger and smaller bedforms, such as sandbanks with wavelengths of several kilometers and (mega-)ripples with wavelengths of decimeters to several tens of meters. This occurs, for example, on the Scotian Shelf (Li and King, 2007), in the southern North Sea (Bellec et al., 2010) and in the northern South China sea (Zhou et al., 2018).

Tidal sand waves are dredged when they become hazardous for navigation (Katoh et al., 1998; Dorst et al., 2011). Frequently, they are also removed as part of sand mining operations (Van Lancker et al., 2010) or installation of offshore structures, such as wind farms (Coates et al., 2015). Little is known about the morphodynamic response to dredging. This brings up the questions: do sand waves regenerate after a dredging event? And if so, on what time scales? And if not, why not? Answering these questions will help optimise dredging activities in navigation channels and wind farms and improve understanding of the impact of these activities on benthic communities that live among tidal sand waves (Cheng et al., 2021; Wyns et al., 2021).

Observations of sand waves after dredging are scarce, but analysis of field data by Katoh et al. (1998) in the Seto Inland Sea (Japan) suggests recovery of tidal sand waves within a period of approximately 10 years. Furthermore, field data in the Rotterdam-Eurogeul and Amsterdam-IJgeul, two navigation channels in the North Sea, point to regeneration of tidal sand waves within several years (Dorst et al., 2011). Campmans et al. (2021), using a highly idealised process-based model, found that sand waves tend to recover after dredging and proposed that the recovery timescale is a function of both the dredged volume and the dredging strategy. However, their model results have not yet been compared with observations, and the scarcity of such observations raises

* Corresponding author.
E-mail addresses: j.m.krabbendam@uu.nl (J.M. Krabbendam), marc.roche@economie.fgov.be (M. Roche), h.e.deswart@uu.nl (H.E. De Swart).

https://doi.org/10.1016/j.margeo.2022.106866
Received 26 April 2022; Received in revised form 27 June 2022; Accepted 12 July 2022
Available online 19 July 2022

the question whether this is generally the case. In this study, bathymetric surveys, that have been conducted every few years using multibeam echosounders in areas previously subject to sand extraction in the Belgian part of the North Sea, are analysed to investigate whether tidal sand waves regenerated after they had been dredged. This analysis shows that this is not so evident.

Section 2 starts with a description of the study areas, followed by a description of the multibeam echosounder data and the methodology to analyse these in Section 3. Results will be presented in Section 4 and discussed in Section 5. The conclusions are given in Section 6.

2. Study areas

The area studied comprises the Kwinte Bank and Buiten Ratel, two of the large-scale Flemish banks on the Belgian continental shelf (Fig. 1). Both sandbanks are covered by sand waves and (mega-)ripples (small to large dunes). Here, the semi-diurnal M_2-tide is dominant with depth-averaged velocity amplitudes of about 0.7–0.75 m/s and an ellipticity of approximately 0.2 (obtained from the model ZUNO, for details see e.g. Zijl, 2013). The joint action with S_2 (depth-averaged amplitude of 0.2 m/s) causes spring-neap cycles, with maximum spring-flood currents of about 1 m/s. The spring-neap cycles are also visible in the tidal range which is about 5 m during spring and 3 m during neap tide.

Since the 1970s, sand has been extracted from multiple parts of these banks. This study considers three sites that have been closed to mining activities (Roche et al., 2017). Two areas (KBMA and KBMB) are located on the Kwinte Bank, where the largest amount of sand has been removed (Degrendele et al., 2010) resulting in the formation of two depressions: the 'central depression' in KBMA and the 'northern depression' in KBMB (Fig. 1 (c)-(d)). In the central depression, the average depth is about 15–16 m with respect to Lowest Astronomical Tide (LAT), in the northern depression the average depth is 19–20 m LAT. Both depressions are approximately 5 m deeper than its surroundings. The KBMA and KBMB areas were closed to extraction in 2003 and 2010, respectively. The third site (BRMC) is located on the Buiten Ratel sandbank. On BRMC, sand extraction took place mainly between 2008 and 2014, which has lowered the average depth to a level of 22–23 m LAT. The BRMC area was closed to extraction in early 2015 (Roche et al., 2017). This area will be called the 'western depression' from now on (Fig. 1 (e)). The three depressions are the focus of this study.

The sand in the central depression has a median grain size d_{50} of 300–350 μm, is moderately-poorly sorted and contains shell fragments (De Backer et al., 2011). The sand in this depression is distinctively different from the rest of KBMA (Bellec et al., 2010). In the northern and western depression, the sand is coarser with median grain sizes of 350–400 μm (De Backer et al., 2011) and 350–450 μm, respectively (De Backer et al., 2017). In these areas, extraction caused near-complete depletion of the Holocene top layers (0–2 m left) (Degrendele et al., 2017). In KBMA, however, a thickness of 1–3 m remained and this area has been reopened to sand extraction since January 1st 2021 (Degrendele et al., 2021). The layer below the Holocene top layer consists of Quaternary deposits of varying origins: coastal, fluvial, lagoon and marsh-type deposits which are not all sandy in nature (Bellec et al., 2010).

3. Materials and methods

3.1. Multibeam echosounder data

In KBMA, bathymetric data obtained during 31 surveys that took place in the period 2000–2019 were analysed, in KBMB 30 surveys from the period 2003–2019 and in BRMC 18 surveys from 2010 to 2019 (for further details see Supporting Information (SI), Table S1). Bathymetric data were obtained with two generations of the Kongsberg multibeam echosounders (MBES): the RV Belgica 100 kHz EM1002 in the period 2000–2008 and the RV Belgica 300 kHz EM3002 dual from 2009 to

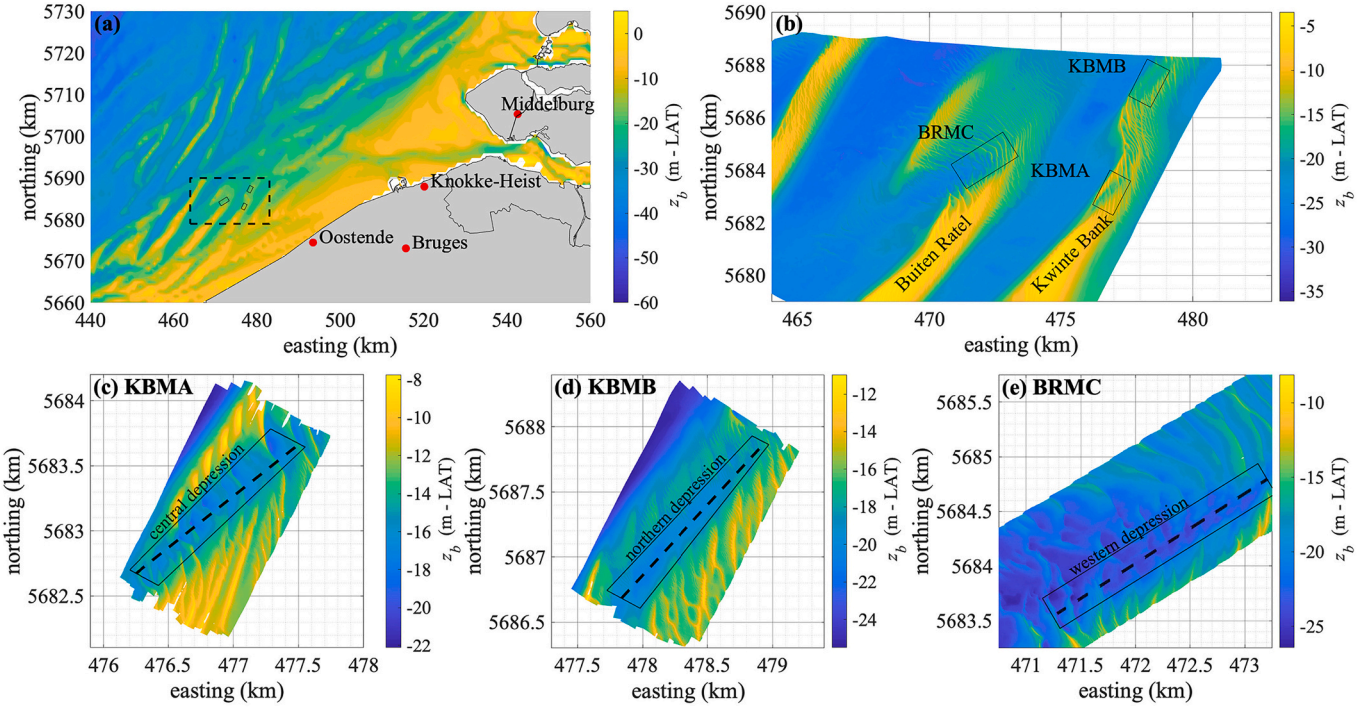

Fig. 1. (a) Location of study areas, bathymetry from EMODnet 2020. (b) zoom-in of dashed box in panel (a), reference bed level from 2000 to 2002 (source: Continental Shelf Service, Federal Public Service Economy, 2022). (c)-(e) zoom-ins of KBMA, KBMB and BRMC (obtained 19 September - 25 November 2019, source: Continental Shelf Service, Federal Public Service Economy, 2022) with location of the transects of interest (black dashed lines) and depressions (the areas most affected by extraction; black solid lines). Note the different colorbars. (For interpretation of the references to colour in this figure legend, the reader is referred to the web version of this article.)

2020 (Roche et al., 2017). Both generations of MBES are compliant with the IHO-S44 standard: the EM1002 has standard Order 1 with an uncertainty of ±0.6 m at depths of 20 m, and the EM3002 has the standard Special order, with an uncertainty of ±0.3 m at depths of 20 m. Roll, heave and heading corrections happened real time using a Seatex MRU5 motion sensor and an Anschutz Standard 20 gyrocompas. Data were corrected for the tide with a tidal reduction method using tide gauge data obtained from multiple stations along the Belgian Coast (Degrendele et al., 2010). Different GPS positioning systems were used: Sercel NR103 (uncertainty <5 m) for the EM1002 time series and a Thales Aquarius 02 (decimetric uncertainty) for the EM3002 dual dataset.

Multibeam echosounder measurements also provide an acoustic backscatter signal, which measures the intensity of the acoustic energy scattered back to the receiving sonar antenna. For a given angle of incidence, the backscatter strength varies with the nature of the seabed: hard, rough bottoms made up of coarse sediments return much more energy than smoother, soft bottoms made up of fine sediments. For this reason, over the past two decades, the backscatter has been used more and more as a proxy to characterise the seabed nature (Lurton et al., 2015). It is not straightforward to compare backscatter signals obtained with different uncalibrated MBES and therefore only backscatter from the EM3002 dual dataset are included in the analysis. These signals were corrected for level attenuation and instantaneous insonified area. The acoustic signal within the angular interval ±[30°, 50°] that best reflects the nature of the sediment, is interpolated on a grid. These signals are hereafter averaged over a geographical area, so that time variations of these averages reflect a change of the seafloor. This standardised method of processing backscatter signals is described in detail in Roche et al. (2018).

3.2. Analysis

The bathymetric models derived from the multibeam echo soundings have a resolution of 1 × 1 m and highlight bedforms of different dimensions (Continental Shelf Service, Federal Public Service Economy, 2022). In order to isolate the tidal sand waves, these data were processed in a way similar to Van Dijk et al. (2008) and Cazenave et al. (2013). For both KBMA, KBMB and BRMC, a fixed grid was defined and data from every survey were interpolated on this grid, to ensure a constant domain size. Data gaps were filled using 2D linear interpolation to obtain bed levels z_b in m at each grid point. A 2D tapered cosine window with lobes of 10% of the domain length in each direction was applied before taking the 2D Fourier transform to suppress the effect of the edges. Hereafter, a fourth order, high-pass Butterworth filter was applied in the wave number space, so that all bedforms with wavelengths λ smaller than 50 m are retained ($\lambda_{cutoff} = 50$ m). These bedforms are assumed to be (mega-)ripples h_{mr} in m. This high-pass bed level signal was subsequently subtracted from z_b, so that the result contains only the tidal sand waves and sandbanks (h_{sbsw} in m). Hereafter, the h_{mr} topography was no longer considered. This resulting h_{sbsw} was interpolated on three transects, drawn in the depressions (Fig. 1); additional transects are considered in the SI (Fig. S1). These transects are chosen in such a way, that they are oriented perpendicular to the sand wave crests. Along these transects, sandbanks (h_{sb}) were removed using a Gaussian moving-average window with a size of 400 m, which is twice the average sand wavelength. This resulted in sand wave topography h_{sw} (m). An overview of the methodology applied to obtain h_{sw} from the bathymetric models is provided in Fig. 2. The root-mean-square wave height h_{rms} (m) was calculated from h_{sw} as:

$$h_{rms} = \sqrt{\overline{h_{sw}^2}} \tag{1}$$

where the bar indicates averaging, i.e. $\frac{1}{L_x}\int \cdot dx$, along a transect with length L_x and x the along-transect coordinate. The crest (V_c) and trough volumes (V_t) are as follows;

$$V_c(t) = \int_0^{L_x} h_{crest}(t,x)dx \quad V_t(t) = -\int_0^{L_x} h_{trough}(t,x)dx \tag{2}$$

where $h_{crest} = (h_{sw} > 0)$ and $h_{trough} = (h_{sw} < 0)$. These volumes are interpreted as bed level volumes per unit width (m^3/m, see also the shaded areas in Fig. 3). Along each transect, unfiltered data are used to compute the average bed level $\overline{z_b}$ (m - LAT) to investigate trends in background bathymetry. The unfiltered bed level variance σ^2 (m^2) is computed to consider temporal changes in tidal sand waves and mega-ripples combined.

4. Results

Fig. 3 (a) shows the sand wave topography h_{sw} as a function of distance x (m) along the transect in the central depression at March 3rd 2003 and November 25th 2019; Fig. 3 (b) shows h_{sw} in colors as a

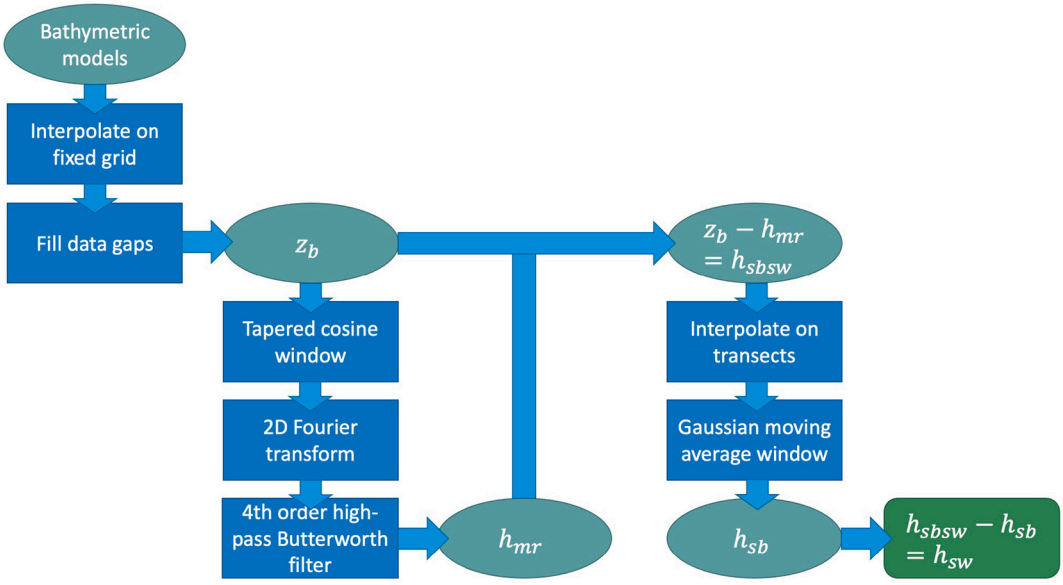

Fig. 2. Methodology to obtain bed levels z_b, (mega-)ripple h_{mr}, sandbank h_{sb} and sand wave topographies h_{sw} (m) from bathymetric models using interpolation, filtering of the 2D Fourier transform and applying a moving average window.

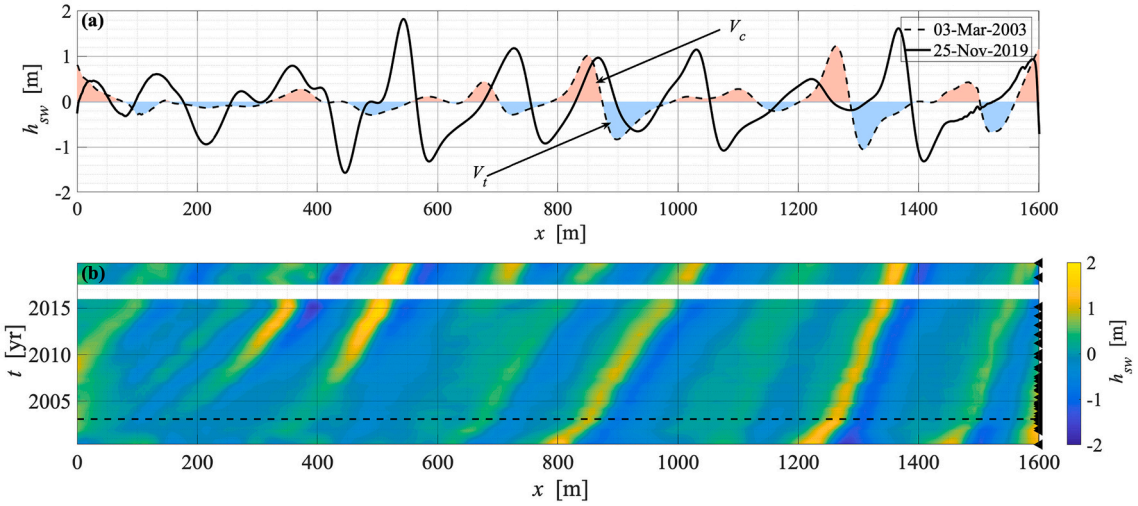

Fig. 3. (a) Sand wave topography h_{sw} (m) as a function of distance x (m) along a transect located in the central depression in KBMA obtained on March 3rd 2003 (dashed line) and November 25th 2019 (solid line). The red and blue shaded areas denote crest- and trough volumes V_c and V_t, respectively (see Section 3.2). (b) Color plots of sand wave topographies h_{sw} (m) as a function of time t (yr) and distance x (m). The dashed line corresponds to the closure of KBMA to sand extraction, and the black triangles at $x = 1600$ m indicate when surveys took place. The color plot is interrupted due to a data gap between 2015 and 2018. (For interpretation of the references to colour in this figure legend, the reader is referred to the web version of this article.)

function of both x and time t (yr). This color plot is interrupted due a 3-year data gap in the period 2015–2018, as is made visible by the black triangles to the right that mark the survey dates. The shaded areas in panel (a) correspond to V_c and V_t as described in Section 3.2. Just after closure of the area to sand extraction in 2003, the height of the sand waves is small, especially in the first 800 m of the domain. As from 2008, however, crests (yellow colors) and troughs (blue colors) start to appear (Fig. 3 (b)) with an average wavelength (crest-to-crest distance) of approximately 160 m, indicating sand wave growth. As a result, the profile of 2019 shows new sand waves between $x = 0$ m and $x = 800$ m. The sand waves in the second half of the transect are more or less constant in height, but their migration rate (position of crests in (x, t)-diagram) decreased from 14 to 15 m/yr to 8–9 m/yr after closure to extraction.

Unlike the sand waves in the central depression, those in the northern depression do not recover during the measurement period (Fig. 4). There are no clear sand waves left after the extraction stopped in 2010; and no increase in h_{sw} is observed. The profile obtained in 2019 shows even less variation than in 2010. The small peak located at $x = 1300$ m in 2003 migrates with a nearly constant velocity of 6 m/yr.

Similarly, the sand wave height in the western depression decreased rapidly in the years prior to the closure of BRMC and no changes are visible in the period 2015–2019 (Fig. 5). The profiles obtained in 2014 and 2019 are merely shifted horizontally along the transect. The average wavelength along this transect is approximately 155 m and the migration rate is fairly constant at 0–2 m/yr.

Figs. 6 (a) shows the root-mean square wave height h_{rms} along each transect as a function of time. In all three cases, h_{rms} decreased prior to the closure of the sites (dashed, coloured lines). In the northern and western depression, h_{rms} was constant after closure at 0.2 m and 0.7 m, respectively (red and green scatters). In the central depression, h_{rms} increased from 0.4 m in 2008 to 0.65 m in 2019 (blue scatters).

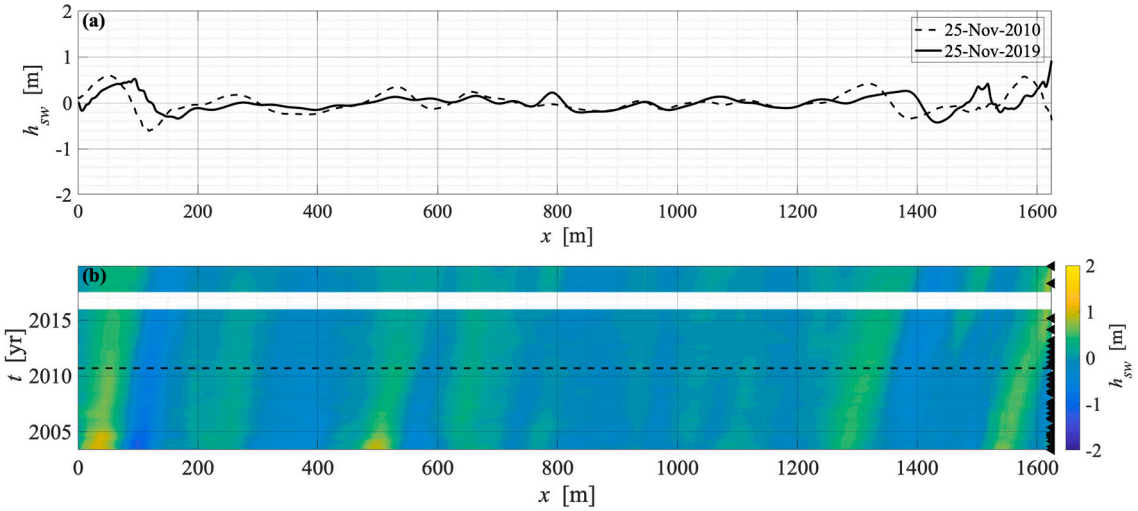

Fig. 4. (a) Sand wave topography h_{sw} (m) as a function of distance x (m) along a transect located in the northern depression in KBMB obtained on November 25th 2010 (dashed line) and November 25th 2019 (solid line). (b) Color plots of sand wave topography h_{sw} (m) as a function of time t (yr) and distance x (m). The dashed line corresponds to the closure of KBMB to sand extraction, and the black triangles at $x = 1630$ m indicate when surveys took place. The color plot is interrupted due to a data gap between 2015 and 2018. (For interpretation of the references to colour in this figure legend, the reader is referred to the web version of this article.)

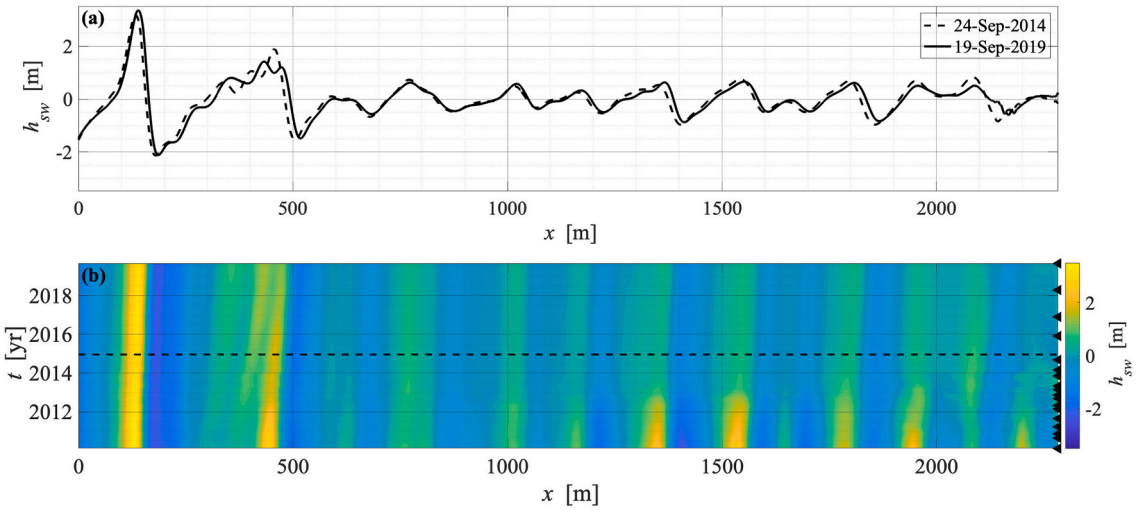

Fig. 5. (a) Sand wave topography h_{sw} (m) as a function of distance x (m) along a transect located in the western depression in BRMC obtained on September 24th 2014 (dashed line) and September 19th 2019 (solid line). (b) Color plots of sand wave topography h_{sw} (m) as a function of time t (yr) and distance x (m). The dashed line corresponds to the closure of BRMC to sand extraction, and the black triangles at $x = 2300$ m indicate when surveys took place. (For interpretation of the references to colour in this figure legend, the reader is referred to the web version of this article.)

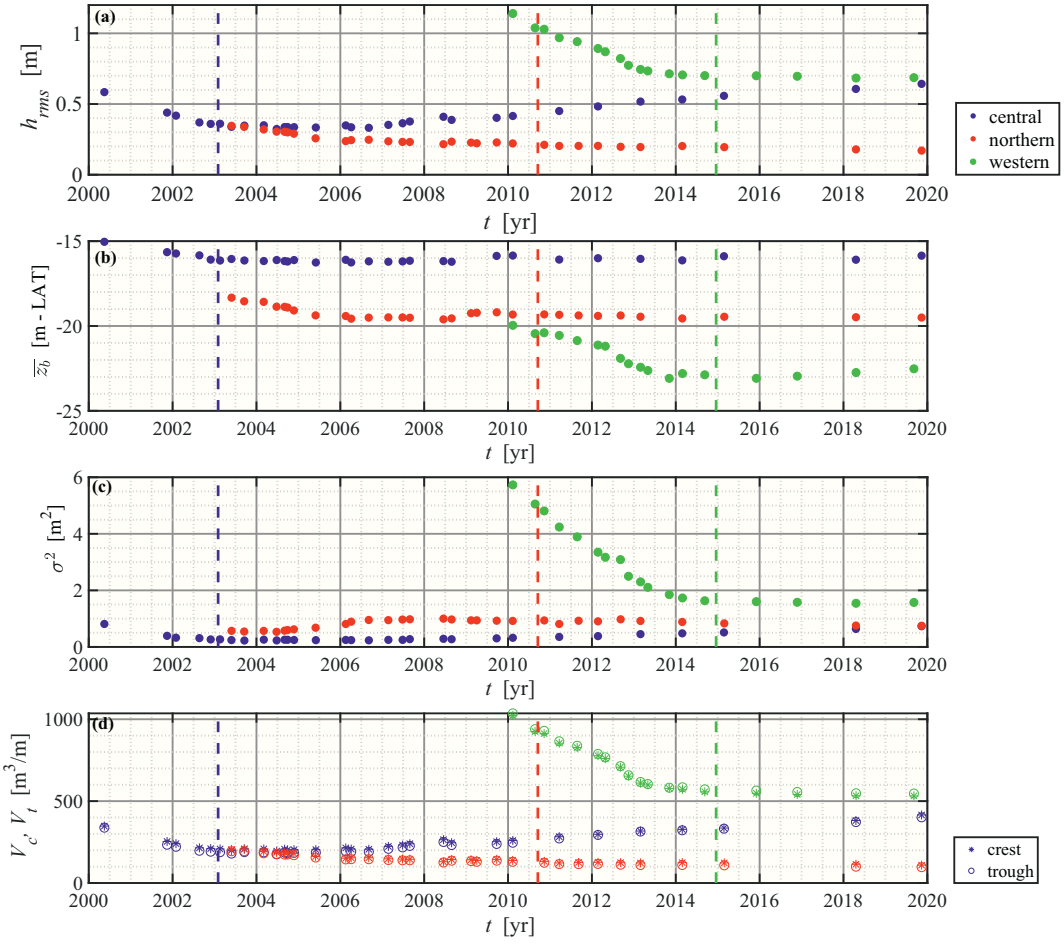

Fig. 6. The root-mean-square bed level h_{rms} (m) (a), the average bed level $\overline{z_b}$ (m - LAT) (b), the bed level variance σ^2 (m^2) (c) and crest and trough volume V_c and V_t (m^3/m, asterisks and circles, respectively) (d) as a function of time t (yr) along transects in the central, northern and western depression (blue, red and green scatters, respectively). The coloured dashed lines in both panels corresponds to the closure to sand extraction. (For interpretation of the references to colour in this figure legend, the reader is referred to the web version of this article.)

The mean water depth $\overline{z_b}$ (m - LAT) along the transects in the depressions decreased up to the moment of closure to extraction, but did not change after (Fig. 6 (b)), suggesting that the depressions caused by sand extraction are not being filled (yet). This is supported by the evolution of the bed level variance σ^2 (m^2) over time (Fig. 6 (c)). In the northern and western depressions, σ^2 remained constant since closure, while there was a slight increase in the central depression, reflecting the sand wave growth. The sand waves just to the southeast and northwest of the depressions, show the same trends: both the average bed level and the variance did not change (SI, Figs. S2-S7). The crest and trough volumes V_c and V_t per m width (m^3/m) evolved in the same way: both decreased prior to closure (Fig. 6 (d)). Only in the central depression did these volumes increase again after 2008, indicating that troughs were deepening and crests were growing at the same rates. In the northern and western depression, both volumes remained constant after closure.

Fig. 7 shows that there is a persistent difference in backscatter signal between the central depression (blue shaded area) and that in the sand wave fields just to the north (green shaded area) and to the south (yellow shaded area) in KBMA. In the area to the north, the sand is coarser and to the south, it is finer than in the central depression. This difference is stable in time, as is visible in Fig. 7(b). Here, the backscatter signals averaged over the central depression (blue) and areas to the north (green) and south (yellow), respectively, are plotted as a function of time t (yr). The shaded areas correspond to ± one standard deviation. Although there is some overlap in the standard deviations, no significant trend is observed, suggesting a general stability of the nature of the surface sands at the time scale considered.

5. Discussion

Analysis of field data by Katoh et al. (1998) and Dorst et al. (2011) suggested that sand waves will regenerate within a few years after dredging. However, results from the Belgian continental shelf indicate that this is not always so evident. Tidal sand waves in the central depression (KBMA) seemed to reappear approximately 5 years after sand extraction had stopped, but in the northern and western depressions no sign of regrowth was detected during the observational period, which spans, respectively, 9 and 5 years after closure. However, regrowth may become visible in these areas in future surveys. The conclusions are independent of the type of filter, cut-off frequency or the moving average window applied (SI, Figs. S10-S12). The filter affects peaks in the bottom topography by a few decimeters, which results from the removal of the small bedforms.

To explain the differences in sand wave behaviour at the three sites, we made use of available model studies that describe the initial formation of sand waves using linear stability analysis (Besio et al., 2003; Van Santen et al., 2011; Blondeaux and Vittori, 2011; Campmans et al., 2021). This theory assumes that initially there are only small bedforms, whose amplitudes grow or decay exponentially in time, with rates that are independent of their initial amplitude. In the cases studied here, application of this theory is reasonable, because at all sites, sand waves that remained after dredging had heights on the order of 5% of the water depth (Figs. 3-5, panels (a)). These studies revealed that differences in growth rates are attributed to differences in amplitude and ellipticity of the depth-averaged tidal current, water depth, sediment characteristics and availability, and dredging strategy. We present an overview of these characteristics for each site in Table 1. It would be interesting to know the differences in sand waves characteristics prior to dredging, but unfortunately, these data do not exist for the Kwinte Bank.

Tidal characteristics at the three sites are very similar according to the ZUNO model, and it is therefore not likely that they explain the different responses to dredging. However, in these areas, the ZUNO grid size is about 1000 m (Zijl, 2013). Observations obtained by Garel (2010) indicate that the current in the central depression is canalised in the

Table 1
Overview of environmental and sand wave characteristics for each of the depression areas.

	Central depression	Northern depression	Western depression
Environmental characteristics			
Mean water depth (post-dredging)	15–16 m LAT	19–20 m LAT	22–23 m LAT
Median grain size	300–350 μm	350–400 μm	350–450 μm
Depth averaged velocity amplitude	0.7–1 m/s	0.7–1 m/s	0.7–1 m/s
Remaining thickness of Holocene sand	1–3 m	0–2 m	0–2 m
Dredging period	1970s-2003	1970s-2010	2008–2015
Sand wave characteristics			
Mean wavelength (post-dredging)	160 m	–	155 m
Mean migration speed (post-dredging)	8–9 m/yr	6 m/yr	0–2 m/yr
h_{rms} (post-dredging)	0.4 m	0.2 m	0.7 m
h_{rms} in 2019	0.65 m	0.2 m	0.7 m

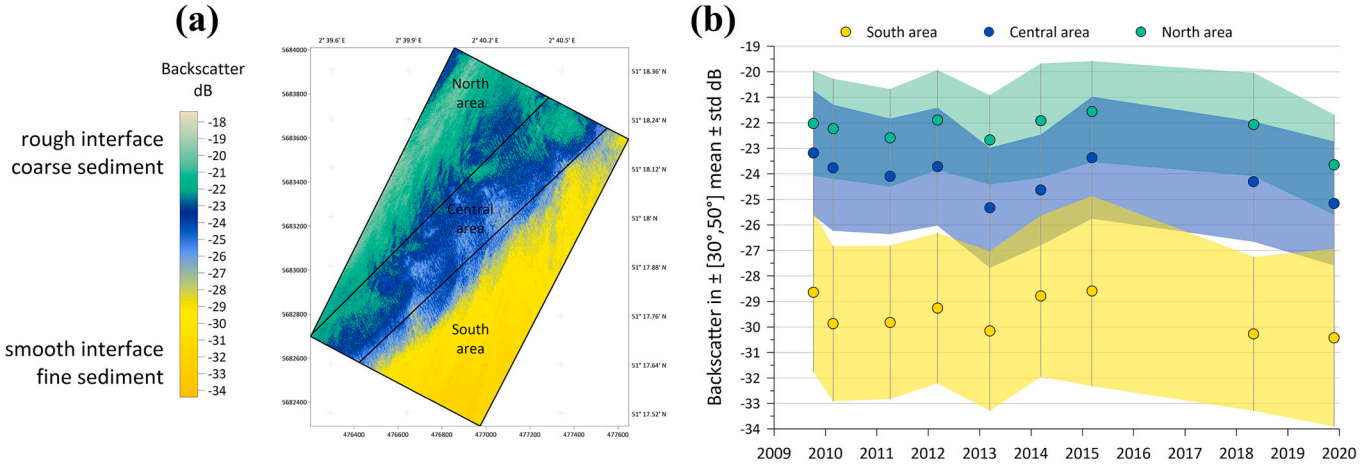

Fig. 7. (a) Backscatter signals in angular range ±[30°, 50°] obtained in KBMA are averaged over the central depression (blue) and the areas to the north (green) and south (yellow). (b) Averaged signals as a function of time t (yr) (colored dots) ± one standard deviation (shaded areas). (For interpretation of the references to colour in this figure legend, the reader is referred to the web version of this article.)

sense that the main axis of the tidal ellipse is oriented along the depression. Although these observations were taken over only a couple of days, they seem to indicate that the tidal currents might be slightly enhanced compared to measurements obtained just outside of the depression. To test what effect this could have, we performed simulations with the model of Besio et al. (2003), which is a local, linear model describing the initial growth of tidal sand waves on a horizontal flat seabed. Using the measured water depth, grain size and tidal flow characteristics for the central depression, the model predicts an e-folding time scale (the time necessary to increase the amplitude with a factor e) of a couple of years. A 5% increase of the depth-averaged current amplitude while keeping the rest of the parameters constant, leads to a decrease of the e-folding time scale with 25%. This may be one of the reasons why growth rates are larger in KBMA. Hydrodynamic measurements were not obtained in the other two areas.

Campmans et al. (2021) have shown that the recovery time may be a function of the dredged volume and the time between successive dredging events. In the years prior to closure, the yearly sand extraction rate standardised by surface area is highest for BRMC (Degrendele et al., 2010; Roche et al., 2017). However, the KBMA and KBMB exact extraction rates before 1999 are unknown and by this point the central and northern depression had already formed. It is therefore difficult to draw conclusions from the extraction rates.

The mean depths and grain sizes at the three sites are quite different, so they might explain the differences in response to dredging. Experiments with the model of Besio et al. (2003) show that a change in water depth has a much larger influence on the initial growth than a change in grain size. The e-folding time scale doubled and tripled if the water depth changed from the one from the central depression to the one of the northern (+4 m) or western depression (+7 m), respectively, while changes in grain size yielded changes in the e-folding time scale of approximately 10%. Besides the enhanced growth in shallower water due to stronger tidal bottom stress, the bed is also more prone to wind- and wave action in shallower water. This has the potential to mobilise more sand, as has been demonstrated by Campmans et al. (2017).

The local sediment availability is quite different between the three areas: the central depression is the only site where part of the sandy Holocene top layer remains. In the northern and western depression, the Pleistocene deposits have reached the surface (Degrendele et al., 2021). These deposits have not been studied in detail for these areas, but they have been for the central depression and the nearby Middelkerke Bank. Trentesaux et al. (1999) and Bellec et al. (2010) showed that these deposits may consist of very different materials. Besides, these sediments are assumed to be so compact that their critical shear stress for initiation of motion is larger than the maximum shear stress induced by the local water motion. Thus, there is probably no sufficient local source of erodible sand at the bed in the northern and the western depression.

In principle, sand could be transported into the depressions from surrounding areas and result in sand wave growth. Terseleer et al. (2016) indicated that this happened during the extraction period in BRMC. However, results from the KBMA area indicate that this does not happen, as there is no change in average bed level both in- and outside the central depression (Fig. S3), nor in the sand wave topography of the neighboring sand wave fields (Fig. S2). The width of the sand wave field to the northwest of the central depression did decrease somewhat (Fig. S8), but the backscatter signal in the central depression did not change over time (Fig. 7). This signal is expected to change if the sand from the northwest ended up in here as this sand has a significantly larger median grain size (see also Bellec et al., 2010). Therefore, we conclude that the growth of the sand waves in the central depression is probably the result of the local redistribution of sand: it is eroded in the troughs and deposited at the crests, which is fully in line with the free instability concept.

Several studies have looked at the effects of limited sediment availability on the formation of bedforms in a unidirectional current (Porcile et al., 2020; Jarvis et al., 2022) and in oscillatory currents (Blondeaux et al., 2016). They show that, initially, there are no differences in the formation. Once the height of the bedforms approaches the thickness of the sediment layer, however, their length tends to increase, their height to decrease and their shape becomes more three dimensional compared to the case with unlimited availability of sand. The monitoring of both the northern and western depression is still ongoing, so in the future it might be possible to observe regeneration in these areas as well. Then, the influence of local sediment availability may be visible from sand wave shape changes. These observations could be used to derive a relation between recovery time and environmental parameters such as water depth, characteristics of the bed and of the tide, which could be helpful for optimizing dredging and sand extraction strategies in the future.

6. Conclusions

Little is known about the response of tidal sand waves after dredging, but the few available studies assume that they will recover within a few years. To further explore this, multibeam data of three areas on the Flemish banks on the Belgian continental shelf were analysed. These areas were subject to sand extraction that has since been stopped. Using Fourier analysis and filtering techniques, the tidal sand waves were separated from the underlying sandbanks and superimposed (mega-) ripples, so that the sand wave topography along transects could be followed in time. In the central depression (KBMA), tidal sand waves seemed to form approximately 5 years after extraction activities had stopped. In the northern and western depression (KBMB and BRMC), no growth occurred during the observation period, respectively 9 and 5 years after closure. Possible explanations for this difference in response time are differences in mean water depth and local sand availability, both of which slow down the recovery and are significantly different from the central depression. The local availability of erodible sand may play a role, as bed level changes and backscatter timeseries indicate that the regeneration of sand waves in the central depression originates from local reworking processes: the sand is eroded in the troughs and deposited on the crests.

Data availability

The bathymetric data of KBMA, KBMB and BRMC (Continental Shelf Service, Federal Public Service Economy, 2022) are available via Zenodo (DOI https://doi.org/10.5281/zenodo.6394966) with the CC BY-NC-SA 4.0 license (non-commercial use only). The Matlab scripts to separate and analyse tidal sand waves from bathymetric data are available via Figsharehttps://doi.org/10.23644/uu.19453439.v1

Declaration of Competing Interest

The authors declare that they have no known competing financial interests or personal relationships that could have appeared to influence the work reported in this paper.

Acknowledgments

This research is part of the Industrial Doctorates programme with project number NWA.ID.17.038 funded by the Dutch Research Council (NWO).

Appendix A. Supplementary data

Supplementary data to this article can be found online at https://doi.org/10.1016/j.margeo.2022.106866.

References

Ashley, G.M., 1990. Classification of large-scale subaqueous bedforms; a new look at an old problem. J. Sediment. Res. 60, 160–172. https://doi.org/10.2110/jsr.60.160.

Bellec, V.K., Van Lancker, V.R.M., Degrendele, K., Roche, M., Le Bot, S., 2010. Geo-environmental characterization of the Kwinte Bank. J. Coast. Res. 63–76. https://doi.org/10.2112/SI51-006.1.

Besio, G., Blondeaux, P., Frisina, P., 2003. A note on tidally generated sand waves. J. Fluid Mech. 485, 171–190. https://doi.org/10.1017/S0022112003004415.

Besio, G., Blondeaux, P., Brocchini, M., Hulscher, S.J.M.H., Idier, D., Knaapen, M.A.F., Németh, A.A., Roos, P.C., Vittori, G., 2008. The morphodynamics of tidal sand waves: A model overview. Coast. Eng. 55, 657–670. https://doi.org/10.1016/j.coastaleng.2007.11.004.

Blondeaux, P., Vittori, G., 2011. A parameterization of the wavelength of tidal dunes. Earth Surf. Process. Landf. 36, 1152–1161. https://doi.org/10.1002/esp.2137.

Blondeaux, P., Vittori, G., Mazzuoli, M., 2016. Pattern formation in a thin layer of sediment. Mar. Geol. 376, 39–50. https://doi.org/10.1016/j.margeo.2016.03.011.

Campmans, G.H.P., Roos, P.C., De Vriend, H.J., Hulscher, S.J.M.H., 2017. Modeling the influence of storms on sand wave formation: a linear stability approach. Cont. Shelf Res. 137, 103–116. https://doi.org/10.1016/j.csr.2017.02.002.

Campmans, G.H.P., Roos, P.C., Van der Sleen, N.R., Hulscher, S.J.M.H., 2021. Modeling tidal sand wave recovery after dredging: effect of different types of dredging strategies. Coast. Eng. 165, 103862.

Cazenave, P.W., Dix, J.K., Lambkin, D.O., McNeill, L.C., 2013. A method for semi-automated objective quantification of linear bedforms from multi-scale digital elevation models. Earth Surf. Process. Landf. 38, 221–236. https://doi.org/10.1002/esp.3269.

Cheng, C.H., Borsje, B.W., Beauchard, O., O'flynn, S., Ysebaert, T., Soetaert, K., 2021. Small-scale macrobenthic community structure along asymmetrical sand waves in an underwater seascape. Mar. Ecol. 42, e12657 https://doi.org/10.1111/maec.12657.

Coates, D.A., Van Hoey, G., Colson, L., Vincx, M., Vanaverbeke, J., 2015. Rapid macrobenthic recovery after dredging activities in an offshore wind farm in the Belgian part of the North Sea. Hydrobiologia 756, 3–18. https://doi.org/10.1007/s10750-014-2103-2.

Continental Shelf Service, Federal Public Service Economy, 2022. Bathymetric terrain models of KBMA, KBMB and BRMC. KBMB and BRMC. https://doi.org/10.5281/zenodo.6394966.

Damen, J.M., van Dijk, T.A.G.P., Hulscher, S.J.M.H., 2018. Spatially varying environmental properties controlling observed sand wave morphology. J. Geophys. Res. Earth Surf. 123, 262–280. https://doi.org/10.1002/2017JF004322.

De Backer, A., Van Hoey, G., Wittoeck, J., Hostens, K., 2011. Biological Monitoring: Impact of Past and Present Intensive Dredging. Federal Public Service Economy, Belgium, pp. 47–64.

De Backer, A., Breine, N., Hillewaert, H., Pecceu, E., Ranson, J., Van Hoey, G., Wittoeck, J., Hostens, K., 2017. Ecological Assessment of Intense Aggregate Dredging Activity on the Belgian Part of the North Sea. Federal Public Service Economy, Belgium, pp. 47–66.

Degrendele, K., Roche, M., Schotte, P., Van Lancker, V.R.M., Bellec, V.K., Bonne, W.M.I., 2010. Morphological evolution of the Kwinte Bank central depression before and after the cessation of aggregate extraction. J. Coast. Res. 77–86.

Degrendele, K., Roche, M., Vandenreyken, H., 2017. New limits for the sand extraction on the Belgian part of the North Sea? Federal Public Service Economy, Belgium, pp. 135–146.

Degrendele, K., Roche, M., Florian, B., Vandenreyken, H., 2021. The Implementation of the New Reference Level for Sand Extraction on the Belgian Continental Shelf. Federal Public Service Economy, Belgium, pp. 65–76.

Dorst, L.L., Roos, P.C., Hulscher, S.J.M.H., 2011. Spatial differences in sand wave dynamics between the Amsterdam and the Rotterdam region in the Southern North Sea. Cont. Shelf Res. 31, 1096–1105. https://doi.org/10.1016/j.csr.2011.03.015.

Garel, E., 2010. Tidally-averaged currents and bedload transport over the Kwinte Bank, Southern North Sea. J. Coast. Res. 87–94. https://doi.org/10.2112/SI51-008.1.

Jarvis, P.A., Bacik, K.A., Narteau, C., Vriend, N.M., 2022. Coarsening dynamics of 2D subaqueous dunes. J. Geophys. Res. Earth Surf. 127 https://doi.org/10.1029/2021JF006492 e2021JF006492.

Katoh, K., Kume, H., Kuroki, K., Hasegawa, J., 1998. The Development of Sand Waves and the Maintenance of Navigation Channels in the Bisanseto Sea. Coastal Engineering '98 ACSE, Reston, VA, pp. 3490–3502. https://doi.org/10.1061/9780784404119.265.

Li, M.Z., King, E.L., 2007. Multibeam bathymetric investigations of the morphology of sand ridges and associated bedforms and their relation to storm processes, Sable Island Bank, Scotian Shelf. Mar. Geol. 243, 200–228. https://doi.org/10.1016/j.margeo.2007.05.004.

Lurton, X., Lamarche, G., Brown, C., Lucieer, V.L., Rice, G., Schimel, A., Weber, T., 2015. Backscatter Measurements by Seafloor-mapping Sonars: Guidelines and Recommendations. GeoHab Backscatter Working Group.

McCave, I.N., 1971. Sand waves in the North Sea off the coast of Holland. Mar. Geol. 10, 199–225. https://doi.org/10.1016/0025-3227(71)90063-6.

Porcile, G., Blondeaux, P., Colombini, M., 2020. Starved versus alluvial river bedforms: an experimental investigation. Earth Surf. Process. Landf. 45, 1229–1239. https://doi.org/10.1002/esp.4800.

Roche, M., Degrendele, K., Vandenreyken, H., Schotte, P., 2017. Multi time and Space Scale Monitoring of the Sand Extraction and its Impact on the Seabed by Coupling EMS data and MBES Measurements. Federal Public Service Economy, Belgium, pp. 5–38.

Roche, M., Degrendele, K., Vrignaud, C., Loyer, S., Le Bas, T., Augustin, J.M., Lurton, X., 2018. Control of the repeatability of high frequency multibeam echosounder backscatter by using natural reference areas. Mar. Geophys. Res. 39, 89–104. https://doi.org/10.1007/s11001-018-9343-x.

Terseleer, N., Degrendele, K., Roche, M., Van den Eynde, D., Van Lancker, V.R.M., 2016. In: Dynamics of Very-large Dunes in Sandbank Areas Subjected to Marine Aggregate Extraction, Belgian Continental Shelf. Paper presented at Marine and River Dune Dynamics V, 4–6 April 2016, Caernarfon, UK.

Trentesaux, A., Stolk, A., Berne, S., 1999. Sedimentology and stratigraphy of a tidal sand bank in the southern North Sea. Mar. Geol. 159, 253–272. https://doi.org/10.1016/S0025-3227(99)00007-9.

Van Dijk, T.A.G.P., Lindenbergh, R.C., Egberts, P.J.P., 2008. Separating bathymetric data representing multiscale rhythmic bed forms: a geostatistical and spectral method compared. J. Geophys. Res. Earth Surf. 113 https://doi.org/10.1029/2007JF000950.

Van Lancker, V.R.M., Bonne, W.M.I., Garel, E., Degrendele, K., Roche, M., Van den Eynde, D., Bellec, V.K., Brière, C., Collins, M.B., Velegrakis, A.F., 2010. Recommendations for the sustainable exploitation of tidal sandbanks. J. Coast. Res. 151–164. https://doi.org/10.2112/SI51-014.1.

Van Santen, R.B., De Swart, H.E., van Dijk, T.A.G.P., 2011. Sensitivity of tidal sand wavelength to environmental parameters: a combined data analysis and modelling approach. Cont. Shelf Res. 31, 966–978. https://doi.org/10.1016/j.csr.2011.03.003.

Wyns, L., Roche, M., Barette, F., Van Lancker, V.R.M., Degrendele, K., Hostens, K., De Backer, A., 2021. Near-field changes in the seabed and associated macrobenthic communities due to marine aggregate extraction on tidal sandbanks: a spatially explicit bio-physical approach considering geological context and extraction regimes. Cont. Shelf Res. 229, 104546 https://doi.org/10.1016/j.csr.2021.104546.

Zhou, J., Wu, Z., Jin, X., Zhao, D., Cao, Z., Guan, W., 2018. Observations and analysis of giant sand wave fields on the Taiwan Banks, northern South China Sea. Mar. Geol. 406, 132–141. https://doi.org/10.1016/j.margeo.2018.09.015.

Zijl, F., 2013. Development of the Next Generation Dutch Continental Shelf Flood Forecasting Models, Memo, 1205989-003-ZKS-0002. Deltares, Delft.